physchem

MDPI

Review

The Theories of Rubber Elasticity and the Goodness of Their Constitutive Stress–Strain Equations

Vincenzo Villani * and Vito Lavallata

Department of Science, University of Basilicata, Campus Macchia Romana, 85100 Potenza, Italy; lavallata.vito@libero.it

* Correspondence: vincenzo.villani@unibas.it

Abstract: One of the most important challenges in polymer science is a rigorous understanding of the molecular mechanisms of rubber elasticity by relating macroscopic deformation to molecular changes and deriving the constitutive stress–strain equation for the elastomeric network. The models developed from the last century to today describe many aspects of the physics of rubber elasticity; although these theories are successful, they are not complete. In this review we analyze the main theoretical and phenomenological models of rubber elasticity, including their assumptions, main characteristics, and stress–strain equations. Then, we compare the predictions of the theories to our experimental data of polydimethylsiloxane (PDMS) rubber, in order to highlight the goodness of the reviewed models. The nonaffine and phenomenological deformation models verify the experimental curves in tension and compression in the whole investigated deformation range $\lambda \leq 2$. On the contrary, the affine deformation hypothesis is rigorously verified only in the deformation range $\lambda \leq 1$.

Keywords: rubber elasticity models; constitutive stress–strain equations; affine deformation; nonaffine deformation; ideal rubbers; tube models; cross-links; entanglements

Citation: Villani, V.; Lavallata, V. The Theories of Rubber Elasticity and the Goodness of Their Constitutive Stress–Strain Equations. *Physchem* **2024**, *4*, 296–318. https://doi.org/10.3390/physchem4030021

Academic Editor: Francesco Mallamace

Received: 24 June 2024
Revised: 15 August 2024
Accepted: 20 August 2024
Published: 22 August 2024

1. Introduction

Finding the relation between the mechanical and the molecular properties of materials is a long-standing and widely explored task. Despite the progress achieved in this field, there are still open issues to be addressed. The situation becomes complicated in the case of polymer materials, where it is necessary to treat macromolecules consisting of a large number of monomers. This present review analyzes the existing approaches to treating rubber elasticity in terms of the relation between elasticity and the polymer network. The difficulties are discussed: for instance, the non-hierarchical topology of the network leading to enhanced constraints and nonlinearity for large deformations. The most efficient approaches to overcome this are statistical mechanics and molecular dynamics. Furthermore, recent advances are analyzed, taking into account the structure, defects, and connectivity of real rubber networks. Finally, a careful comparison of the respective models with our experimental data are performed.

From the point of view of statistical thermodynamics, linear polymers are long and flexible chains without the structural details of the monomer unit, according to Staudinger's *Makromolekulare Theorie* of 1920 [1]. The Swiss scientist Werner Kuhn was the first to use the Boltzmann entropy equation applied to the statistical thermodynamics of the isolated chain in a dilute solution in 1934, calculating the elastic restoring force of the random coil [2]. Later, in 1946, Kuhn used a statistical macromolecule model to develop the first theory of the entropic elasticity of rubber [3].

To understand the entropic spring behavior of polymer chains, we include the step-by-step detailed derivation of the elastic restoring force of the random coil provided by de Gennes for the fundamental model of the polymer chain on a periodic lattice [4]. The

entropy $S\left(\vec{r}\right)$ associated with the polymer chain is related to the number of conformations (or paths) $N_n\left(\vec{r}\right)$ of n links (or steps) from zero to $\vec{r}$, according to the Boltzmann equation:

$$S\left(\vec{r}\right) = k\log\left(N_n\left(\vec{r}\right)\right)$$

Let us calculate the total number Ω of possible paths on the periodic lattice: if each node has z neighbors (coordination number), the number of distinct possibilities at each step is z and the total number of paths after n steps will be the following:

$$\Omega = \sum_r N_n\left(\vec{r}\right) = z^n$$

The end-to-end vector $\vec{r}$ is the sum of the n step vectors:

$$\vec{r} = \vec{a}_1 + \vec{a}_2 + \ldots + \vec{a}_n = \sum_{i=1}^{n} \vec{a}_i$$

where each term $\vec{a}_i$ is a vector of modulus a with z possible orientations. The vectors have completely independent orientations, and this has important consequences: the root mean square end-to-end distance varies linearly with n:

$$R_0^2 = \left\langle r^2 \right\rangle = \sum_{i,j} \left\langle \vec{a}_i \cdot \vec{a}_j \right\rangle = \sum_i \left\langle a_i^2 \right\rangle = a^2 \cdot n$$

In fact, the cross products cancel each other out:

$$\left\langle \vec{a}_i \cdot \vec{a}_j \right\rangle = \left\langle a_i \cdot a_j \cdot \cos\vartheta_{ij} \right\rangle = a_i \cdot a_j \left\langle \cos\vartheta_{ij} \right\rangle$$

$$i \neq j \left\langle \cos\vartheta_{ij} \right\rangle = 0$$

$$i = j \left\langle \cos\vartheta_{ij} \right\rangle = 1$$

The power law of the random walk size is as follows:

$$R_0^2 = \sum_i a_i^2 = a^2 \cdot n \propto M$$

where M is the molecular weight of the polymer.

The probability distribution function in $\vec{r}$ is defined by the following:

$$p\left(\vec{r}\right) = \frac{N_n\left(\vec{r}\right)}{\sum_r N_n\left(\vec{r}\right)}$$

from which there is the following:

$$N_n\left(\vec{r}\right) = \Omega \cdot p\left(\vec{r}\right)$$

where $p\left(\vec{r}\right)$ is Gaussian if the number of independent steps is large:

$$\exp\left(-\frac{3x^2}{2\langle x^2\rangle}\right) \cdot \exp\left(-\frac{3y^2}{2\langle y^2\rangle}\right) \cdot \exp\left(-\frac{3z^2}{2\langle z^2\rangle}\right) = \exp\left(-\frac{3r^2}{2R_0^2}\right)$$

$$p\left(\vec{r}\right) \propto$$

From the Boltzmann equation, we obtain the change in entropy of the chain for a given elongation:

$$\Delta S\left(\vec{r}\right) = -\frac{3k}{2R_0^2}r^2$$

Entropy decreases quadratically as the elongation increases. For the free energy variation, we have the following:

$$\Delta G\left(\vec{r}\right) = \Delta H\left(\vec{r}\right) - T \cdot \Delta S\left(\vec{r}\right)$$

In the model, the enthalpy H is constant, independently of the conformation of the chain, and therefore cancels out in the free energy difference. We have the fundamental relation as follows:

$$\Delta G\left(\vec{r}\right) = \frac{3k \cdot T}{2R_0^2}r^2$$

As a result, the polymer chain experiences the elastic entropy force:

$$\vec{F}\left(\vec{r}\right) = -\frac{\partial \Delta G}{\partial \vec{r}} = -\frac{3k \cdot T}{R_0^2}\vec{r} \quad (1)$$

The minus sign has a vectorial meaning and indicates that the restoring force is opposite to the deformation. The chain behaves as a linear *entropic spring* whose force constant is proportional to the temperature and inverse to the mean square end-to-end distance and therefore to the chain length and molecular weight [4–6] (Scheme 1).

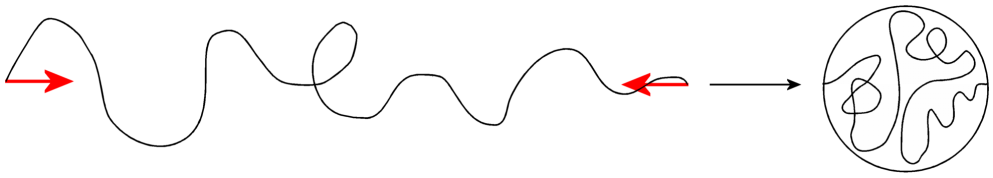

Scheme 1. The stretched low-entropy chain shows a linear restoring force (in red) toward the unstretched high-entropy state: the random coil behaves like an *entropic spring* with an elastic modulus $\frac{3kT}{\langle R^2 \rangle_0}$.

The fundamental aim of a rubber statistical mechanical model is to obtain an equation of state for the macromolecular network, which will describe the stress–strain behavior of rubbers for any deformation, including swelling. Numerous models have been proposed and rigorous statistical mechanical theories describing the mechanical behavior of rubber networks were given in the early 1940s by Kuhn, Flory, Rehner, James, Guth, Wall, Earlier, Treloar, and Mark [7–9].

The current understanding of the molecular mechanism of rubber elasticity is based on two ideal classical theories: the *affine* or *phantom network* models. These linear theories derive the behavior of the rubber from the statistical properties of the isolated chains. In particular, they state that the elastic free energy of a network equals the sum of the elastic free energies of the single chains. More precisely, the interactions between the polymer chains are independent of the state of deformation and do not contribute to the elastic free energy change. In addition, the end-to-end distribution of the network chains is Gaussian, that is, the excluded volume interactions are ignored. Thus, the classical rubber theories are based on the ideal chain, which may pass freely through its neighbors as well as through itself, i.e., the phantom Gaussian chain or random coil [7,8,10].

Experiments demonstrate that the two classical models fail to predict the stress–strain behavior of elastomers at large strain. This has prompted the development of phenomenological theories of continuum mechanics, where only the macroscopic state of the sample is of concern rather than the molecular mechanism [7,11].

Despite their differences, the two ideal molecular models are still useful for the interpretation of experimental data and have formed the basis of more advanced elasticity theories, which take into account the nonlinearity of intermolecular entanglements (topological constraints) among the cross-linked chains (active chains) observed in real networks [7,8,10].

The observed differences between the experiments on real rubbers and the predictions of the classical theories should be attributed to the network defects (including inactive dangling chains and loop structures) and entanglements intrinsic to active chains. The stress softening with increasing tensile strain or swelling is the best-known effect arising from the deformation-dependent contributions from chain entanglements. In fact, around 1970, the role played by entanglements, which result from the chain uncrossability, led to new theoretical models for real rubber networks treating deviations from classical behavior—the *constrained junction*, *slip-link*, and *tube* models [10,12]—and the *real elastic network theory*, which takes into account the presence of isolated defects in a rubber network [13,14].

In agreement with the experimental data, in the entanglement models, trapped entanglements contribute to the free energy change of the stretched network: the reduction in the entropy variation under stretching and therefore in the restoring force would be due to the entanglements on the active chains.

In the constrained junction model, the surrounding chains limit the mobility of active chains and therefore the motion of junction points. According to the constrained junction model, the elastic free energy of the elastomeric network varies between the phantom and the affine models; hence, the properties of the two classical models are bridged if topological constraints are taken into account. For the constrained junction and the slip-link models, due to stretching, there is an increase in the freedom of the chain to fluctuate, since the space available to a chain along the direction of stretch increases.

Different tube models have been developed, such as the affine model of Marrucci [15] and the nonaffine models of Rubinstein and Panyukov [16,17]. Moreover, we will illustrate some notions of the phenomenological theory of Mooney and Rivlin [18,19].

2. Experimental Method

In our previous papers [20–22], rheological, mechanical, and dynamic mechanical experiments were performed and modeled. Now, we prepared an optimal end-linked PDMS rubber (Scheme 2) and the experimental stress–strain curves were compared with the corresponding theoretical equations of the reviewed theories.

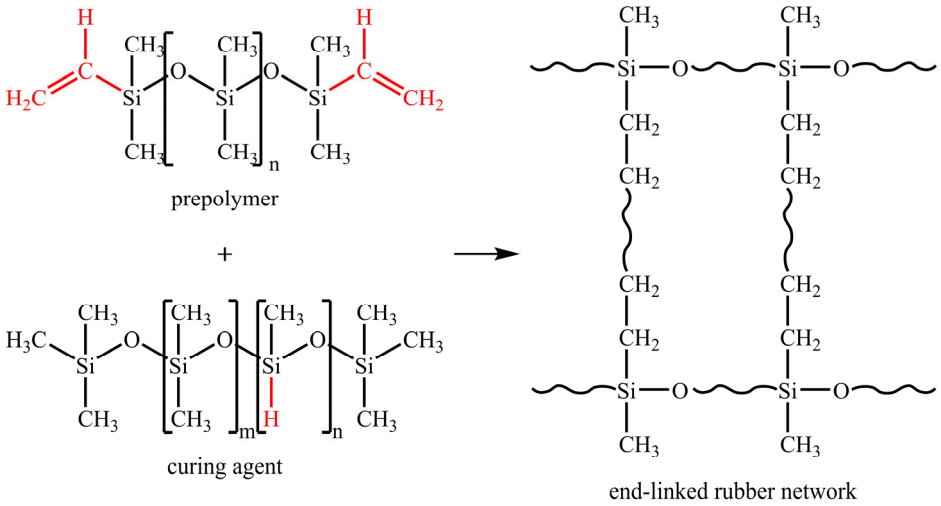

Scheme 2. The molecular structures of the vinyl-terminated prepolymer (**on the top left**), hydride-substituted curing agent (**on the bottom left**), and three-dimensional end-linked network of PDMS rubber (**on the right**) are shown. The reactive groups (in red) are reported.

A PDMS liquid elastomer (Dow Corning Sylgard) medium-viscosity LE-M, as defined in previous papers [20,21], was considered. The LE-M rubber was obtained using a 10:1 weight ratio of prepolymer to curing agent at 30 °C, as recommended.

In a previous paper [20], we determined that the LE-M polymer liquid has a zero-shear rate viscosity $\eta_0 = 5.1\ Pa \cdot s$ and an average number of molecular weight $M_n = 43,100$ unified atomic mass units, with $n = 309$ monomers of –Si$(CH_3)_2$O–. Since $M_n > M_c$, where $M_c = 21,000 - 33,000$, this is the critical molecular weight for the PDMS [21]. LE-M is a viscoelastic polymer melt with an entangled chain. For the PDMS, the entanglement molecular weight M_e [23] is related to M_c as $M_e = \frac{M_c}{2.4}$; consequently, the entanglement density per chain $\nu = \frac{M_n}{M_e}$ of the LE-M polymer melt is included in the range ν = 3–5.

A Q800 dynamic mechanical analyzer (TA Instruments, New Castle, DL, USA) was used and the isothermal experiments at 30 °C were performed, characterizing the LE-M rubber in both compression and tension by means of accurate stress–strain curves at a 5×10^{-4} min^{-1} strain rate. The amplitude of the stress–strain curves was investigated to the best of experimental possibilities up to $\lambda \leq 2$ in tension mode and up to $\lambda \leq 1$ in compression mode.

In order to compare the constitutive stress–strain equations of the reviewed models, a nonlinear regression analysis of the experimental curves was performed. In this way, it was possible to corroborate and highlight the efficiency of the elasticity models of the rubber behavior in tension and in compression experiments. This present study may stimulate further investigations where the cross-linking density, temperature, amplitude, and strain rate in the stress–strain curves are varied systematically.

3. Molecular and Phenomenological Models

3.1. The Affine Network Model

In the *Affine network* model proposed by Kuhn, Wall, and Flory [3,7,24,25], it is assumed that the rubber network consists of independent random coils and the ends of the active chains are rigidly attached to an *elastic background* (i.e., the continuum space for taking into account the macroscopic deformation until the molecular scale), which deforms *affinely* (i.e., the macroscopic deformation applied on the body is translated uniformly to the microscopic level) (Scheme 3). Then, the average positions and fluctuation amplitudes of the junctions change affinely with macroscopic deformation.

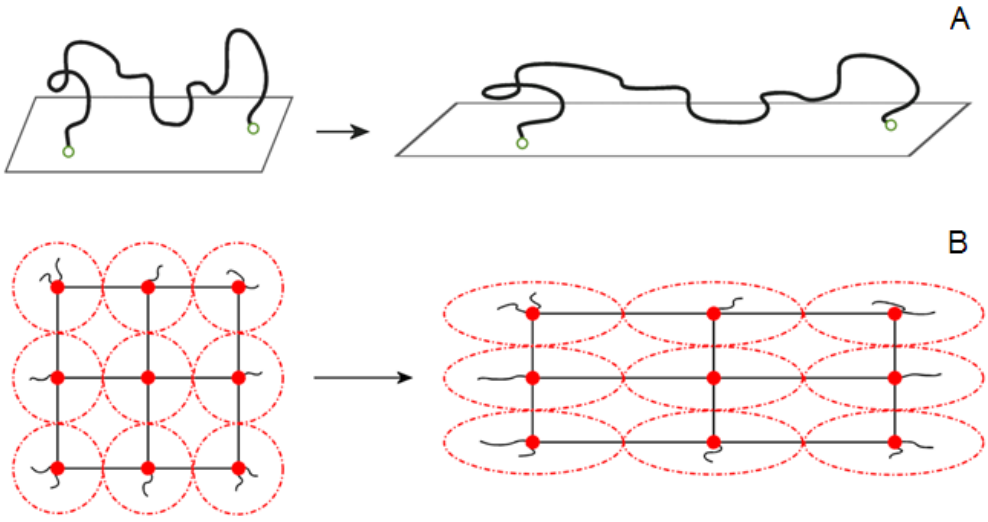

Scheme 3. Picture of the *affine network model*. At the top, the ends (green circles) of an active chain (black line) are connected to the elastic background (gray parallelogram) that affinely deforms (**A**). Below, the isotropic fluctuation amplitudes of the junctions deform in an ellipsoidal affine way filling the space without overlaps (**B**). The affine deformations $\lambda_x = 2$ and $\lambda_y = \lambda_z = 1/\sqrt{2}$ were applied.

In uniaxial stretching, $\lambda_x = \lambda$. Considering the incompressibility condition $\lambda_y = \lambda_z = \lambda^{-1/2}$ (i.e., ideal rubber with a volume variation $\Delta V = 0$ and a Poisson's ratio $\nu = \frac{1}{2}$), the expression for the engineering stress reads as follows:

$$\sigma_{\text{aff}} = kTv\left(\lambda - \frac{1}{\lambda^2}\right) = G_{\text{aff}}\left(\lambda - \frac{1}{\lambda^2}\right) \quad (2)$$

where v is the density of elastically active chains that deform and store energy upon network deformations.

3.2. Derivation of the Stress–Strain Equation for the Flory Affine Model

To learn more about the Flory affine model, we include the step-by-step detailed derivation [24]. Consider the rubber as a network of N interconnected chains. Since the process of cross-link formation is random, the resulting chains will have random lengths. Thus, the end-to-end vectors will be distributed according to the Gaussian probability density function $p(\vec{r})$ previously calculated for the isolated chain in a dilute solution.

Consider the homogeneous deformation of a rubber cube of side L_0 and volume V_0, where $\alpha_x, \alpha_y, \alpha_z$ are the deformation factors. Assuming that the chains and cross-link points are altered in the stretching process in an affine way, then the chain i characterized by the end-to-end vector $\vec{r}_i$, having components (x_i, y_i, z_i) after the deformation, must have had components $\left(\frac{x_i}{\alpha_x}, \frac{y_i}{\alpha_y}, \frac{z_i}{\alpha_z}\right)$ before the deformation.

The number of chains $N_i(x_i, y_i, z_i)$ having the components of the end-to-end vector between x_i and $x_i + \Delta x$, y_i and $y_i + \Delta y$, and z_i and $z_i + \Delta z$ after the deformation is given by the following:

$$N_i(x_i, y_i, z_i) = N \cdot p\left(\frac{x_i}{\alpha_x}, \frac{y_i}{\alpha_y}, \frac{z_i}{\alpha_z}\right) \cdot \frac{\Delta x \Delta y \Delta z}{\alpha_x \alpha_y \alpha_z}$$

Using the probability density function of the freely jointed chain model, we have the following:

$$N_i(x_i, y_i, z_i) = N \cdot \left(\frac{\beta}{\pi^{\frac{1}{2}}}\right)^3 \cdot \exp\left(-\beta^2\left[\left(\frac{x_i}{\alpha_x}\right)^2 + \left(\frac{y_i}{\alpha_y}\right)^2 + \left(\frac{z_i}{\alpha_z}\right)^2\right]\right) \cdot \frac{\Delta x \Delta y \Delta z}{\alpha_x \alpha_y \alpha_z}$$

Consider the transformation of the distributions by a deformation along the axis of a constant volume factor.

$$N_i(x_i, y_i, z_i) = N \cdot p\left(\frac{x_i}{\alpha_x}, \frac{y_i}{\alpha_y}, \frac{z_i}{\alpha_z}\right) \cdot \frac{\Delta x \Delta y \Delta z}{\alpha_x \alpha_y \alpha_z}$$

Using the probability density function $g(\vec{r})$ of the freely jointed chain model, we have the following:

$$N_i(x_i, y_i, z_i) = N \cdot \left(\frac{\beta}{\pi^{\frac{1}{2}}}\right)^3 \cdot \exp\left(-\beta^2\left[\left(\frac{x_i}{\alpha_x}\right)^2 + \left(\frac{y_i}{\alpha_y}\right)^2 + \left(\frac{z_i}{\alpha_z}\right)^2\right]\right) \cdot \frac{\Delta x \Delta y \Delta z}{\alpha_x \alpha_y \alpha_z}$$

Consider the transformation of distributions $g(x), g(y), g(z)$ by a deformation along the x axis of a constant volume factor $\alpha_x = 4$. Then, $\alpha_x \cdot \alpha_y \cdot \alpha_z = 1$ and $\alpha_y = \alpha_z = \frac{1}{\sqrt{\alpha_x}} = \frac{1}{2}$.

While the x component distribution widens, the y, z component distributions narrow.

To calculate the entropy change associated with the deformation, we will calculate the configurational entropy change involved in the formation of a deformed network structure defined by $\alpha_x, \alpha_y, \alpha_z$, then, subtracting the entropy of the undeformed network, we will obtain the entropy associated with the deformation.

We need to find the probability Ω that a non-cross-linked polymer spontaneously realizes a configuration consistent with the formation of a deformed network having N_i chains in the states (x_i, y_i, z_i), as required by the previous equation. Let us denote by Ω_1

the probability that this condition is satisfied. Furthermore, it is necessary that the n units that give rise to the cross-links are suitably close: let us denote by Ω_2 the probability that this event occurs. Then, the probability that the two conditions are satisfied simultaneously is given by $\Omega = \Omega_1 \cdot \Omega_2$.

The probability that a given chain has the components (x_i, y_i, z_i) in the fields Δx, Δy, and Δz is given by the following:

$$g_i = g(x_i, y_i, z_i)\ \Delta x \Delta y \Delta z$$

Then, the probability that each chain of the entire system satisfies a certain set of coordinates (those associated with a distribution) is given by the product of these factors. Grouping together those with the same coordinates, we have the following:

$$\Pi_i g_i^{n_i}$$

This expression must be multiplied by the number of permutations of the chains on the specified distribution, that is, the number of exchanges that leave the distribution unchanged, obtaining the following:

$$\Omega_1 = n! \Pi_i \frac{g_i^{n_i}}{n_i!}$$

Reworking and moving on to logarithms, we have the following:

$$\ln \Omega_1 = \sum_i n_i \ln \frac{g_i n}{n_i}$$

Substituting the expressions of g_i and n_i found above, we have the following:

$$\ln \Omega_1 = -n \left[\frac{\left(\alpha_x^2 + \alpha_y^2 + \alpha_z^2 - 3 \right)}{2} - \ln\left(\alpha_x \alpha_y \alpha_z \right) \right]$$

The probability that one of the n cross-linking units has another unit nearby within a volume δV (interaction space) is given by the following:

$$(n-1)\frac{\delta V}{V}$$

where V is the total volume.

The probability that another of the $n-2$ remaining units has a new unit nearby will be the following:

$$(n-3)\frac{\delta V}{V}$$

and so on.

The probability that the $\frac{n}{2}$ pairs are paired with each other is then as follows:

$$\Omega_2 = (n-1)\,(n-3)\ \cdots \left(\frac{\delta V}{V} \right)^{\frac{n}{2}}$$

Reworking, we have the following:

$$\ln \Omega_2 = -\frac{n}{2} \ln\left(\alpha_x \alpha_y \alpha_z \right) + \text{constant}$$

where the constant is a term independent of the deformation.

Consequently, from the Boltzmann equation, we obtain the entropy of the formation of the deformed network:

$$S = k \ln \Omega = k(\ln \Omega_1 + \ln \Omega_2) = \text{constant} - \frac{k \cdot n}{2}\left(\alpha_x^2 + \alpha_y^2 + \alpha_z^2 - 3\ln\left(\alpha_x \alpha_y \alpha_z\right)\right)$$

It is noteworthy that the parameter β that characterizes the Gaussian probability distribution and that depends on the chain length (the number of monometric units and the length of the bonds) is not present in the entropy equation. The only quantity that characterizes the network structure is the number of cross-links n.

The deformation entropy is obtained by subtracting the entropy of the deformed network from that of the undeformed network S_0 obtained by $\alpha_x = \alpha_y = \alpha_z = 1$:

$$\Delta S = S - S_0 = -\frac{k \cdot n}{2}\left(\alpha_x^2 + \alpha_y^2 + \alpha_z^2 - 3\ln\left(\alpha_x \alpha_y \alpha_z\right)\right)$$

In particular, for uniaxial deformation at a constant volume, we have the following:

$$\alpha_x \cdot \alpha_y \cdot \alpha_z = 1 \text{ and } \alpha_x = \alpha,\ \alpha_y = \alpha_z = \frac{1}{\sqrt{\alpha}}$$

We then have the following:

$$\Delta S = -\frac{k \cdot n}{2}\left(\alpha^2 + \frac{2}{\alpha} - 3\right)$$

The thermodynamic expression of the spring force for ideal rubber is as follows:

$$F = -T \cdot \left(\frac{\partial S}{\partial L}\right)_{T,V}$$

By definition $L = \alpha L_0$, and so we have the following:

$$F = -\frac{T}{L_0} \cdot \left(\frac{\partial S}{\partial L}\right)_{T,V}$$

We then have the following:

$$\left(\frac{\partial S}{\partial \alpha}\right)_{T,V} \equiv \left(\frac{\partial \Delta S}{\partial \alpha}\right)_{T,V} = -k \cdot n\left(\alpha - \frac{1}{\alpha^2}\right)$$

$$F = \frac{kT \cdot n}{L_0} \cdot \left(\alpha - \frac{1}{\alpha^2}\right)$$

Dividing by the area of initial section of the sample, $\frac{V_0}{L_0} = \frac{V}{L_0}$, we have the elastic stress:

$$\sigma = \frac{RT \cdot n}{V}\left(\alpha - \frac{1}{\alpha^2}\right)$$

where n is in mol.

The equation obtained represents the ideal rubber constitutive stress–strain equation.

We observe the presence of three factors: the temperature dependence RT, the structural factor $\frac{n}{V}$, and the deformation factor $\left(\alpha - \frac{1}{\alpha^2}\right)$. The structural factor represents the density of cross-links and the deformation factor prescribes a nonlinear shape for the stress–strain curve. The linear temperature dependence is experimentally confirmed and the nonlinear stress–strain curve is in good agreement with the experimental data in the low-strain range, in traction up to $\alpha < 4$ and in compression up to $\alpha < 1$. For larger deformations, non-entropic factors intervene, which cause a deviation from the theory [7].

3.3. The Phantom Network Model

The *phantom network* model is one of the pioneering models that considered the effect of the entanglement density on the fluctuations of the chain ends [26–28]. James and Guth also assumed that all junctions at the surface of the network are fixed and deform affinely with macroscopic strain, while all junctions and chains inside the bulk of the network fluctuate around their mean positions.

The mean positions of junctions deform affinely with macroscopic deformation, and the junctions of network chains fluctuate around their mean positions due to thermal motions accounting for the entanglements on network chains. Then, the isotropic amplitude fluctuations are not affected under stretching (Scheme 4).

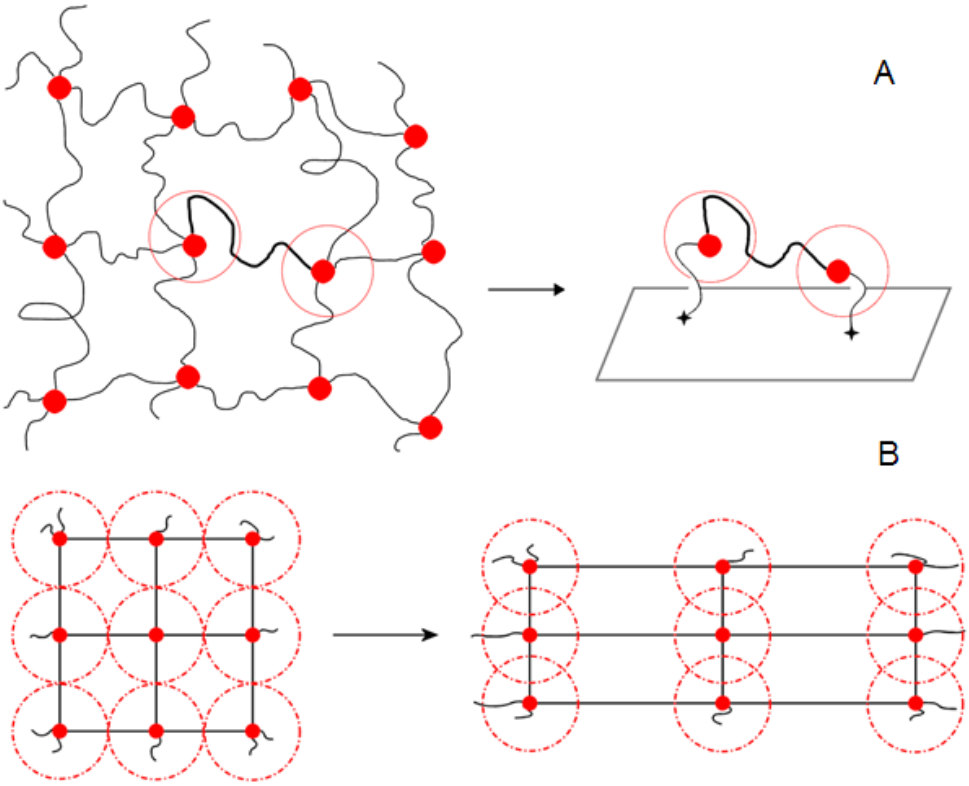

Scheme 4. Picture of the *Phantom network model*. At the top, the effective chains (thin black lines on the right) on the elastomer surface transmit the macroscopic strain to the network bulk (**A**). Below, the lattice deformation is affine; on the contrary, the amplitude of the fluctuations is invariant under stretching and the fluctuations overlap in the transverse direction (**B**). The affine deformations $\lambda_x = 2$ and $\lambda_y = \lambda_z = 1/\sqrt{2}$ have been applied.

The fluctuation amplitude determines how strongly the macroscopic deformation of the network is coupled to the deformation of single chains. Macroscopic deformation is transmitted to the bulk of the network through the effective chains attached to the rubber surface. Therefore, no constraint is imposed on the junctions, whose amplitude is assumed to be independent of the macroscopic extension ratio and chain length. James and Guth assume that the active chains are Gaussian and interact only at the junction points: this means that the network chains can freely move through one another—hence, the *phantom network* model—and the excluded volume effects are neglected in the theory [8,29].

The constitutive equation of the *Phantom network model* in uniaxial stretching is as follows:

$$\sigma_{\mathrm{ph}} = \mathrm{k}Tv\left(\frac{f-2}{f}\right)\left(\lambda - \frac{1}{\lambda^2}\right) = \mathrm{k}T(v-\mu)\left(\lambda - \frac{1}{\lambda^2}\right) = G_{\mathrm{ph}}\left(\lambda - \frac{1}{\lambda^2}\right) \quad (3)$$

where the *functionality* f and the *density of cross-links* μ connect at least three elastically active chains. Then, we have $G_{ph} = C_{ph}G_{aff}$, where $C_{ph} = \frac{f-2}{f}$ is the *elastic effectiveness* of each active chain in the phantom network theory. For high functionalities, the affine and phantom network theories tend to coincide.

Recently, Olsen and Johnson [13,14], based on experimental data from isotopic labeling spectrometry, developed a theory that takes into account the role of defects in the elasticity of the phantom network. The Real *elastic network theory* (RENT) considers the presence of isolated loops of increasing order and dangling ends; in this way, the elastic effectiveness C_{ph} of the network is the average of the elastic effectiveness C_η of different active chains, so $C_{ph} = \langle C_\eta \rangle$ and we also have the following:

$$C_{ph} = \frac{f-2}{f}\left[1 - \frac{2}{f-2}\sum_{l=1}^{\infty} x_l\right] \quad (4)$$

where x_l is the fraction of the lth-order loop.

Lang et al. proposed [30] a convenient way to model cross-link fluctuations in a phantom network, attaching virtual chains of n segments between the ends of the network, strands of N segments, and the affinely deforming non-fluctuating elastic background (Scheme 5). This allows the reduction of a complex network connectivity to a single combined chain, where the fixed end-points of this combined chain deform affinely. The cross-link contribution to elasticity is then written using combined chains of $N + 2n$ segments, as follows:

$$G_c = \frac{N}{N+2n}kTv \quad (5)$$

where only the N segments of the real chain out of the $N + 2n$ segments of the combined chain contribute to stress. The model of cross-link fluctuations provides $G_c \geq G_{ph}$. The situation is different for the models of entangled networks. Here, an entanglement contribution G_e is added to a cross-link contribution G_c; then, $G = G_c + G_e$.

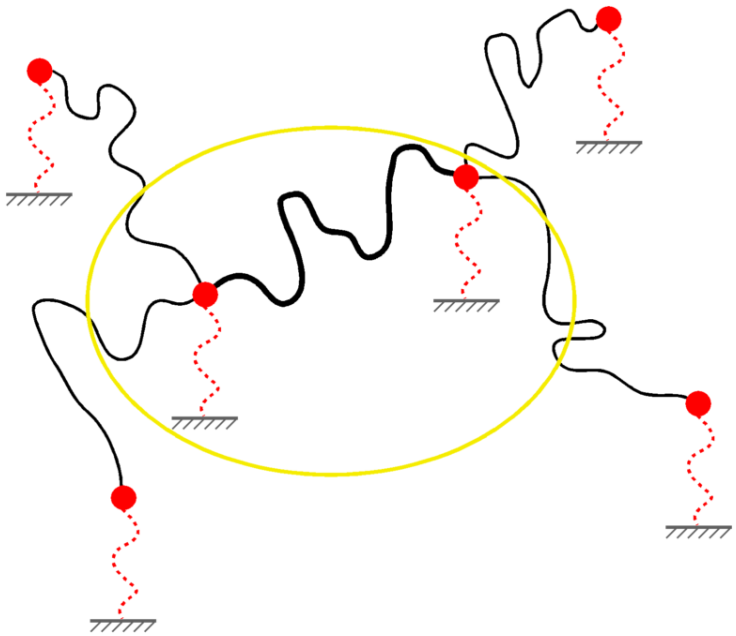

Scheme 5. The *Lang cross-link fluctuation network*. The red dots represent the fluctuating junctions, the thick black line is the probe chain, and the thin black lines show the attached network strands. The dashed red lines are the additional virtual chains that are attached to the non-fluctuating elastic background. A single combined chain (network chain plus two virtual chains) of $N + 2n$ segments is highlighted.

In Figure 1, the constitutive stress–strain equations of the *affine* and *phantom* network models are matched against our experimental data. The phantom and affine models give a good qualitative picture of rubber elasticity, and they are satisfactory at very low and low extension ratios, respectively. However, neither of the two models is able to account for the behavior observed at a higher strain. At a low deformation, a rubber exhibits properties between those of the phantom and affine models, since the extent of the fluctuations should depend on macroscopic strain, being less in the unstretched network and more in the deformed network.

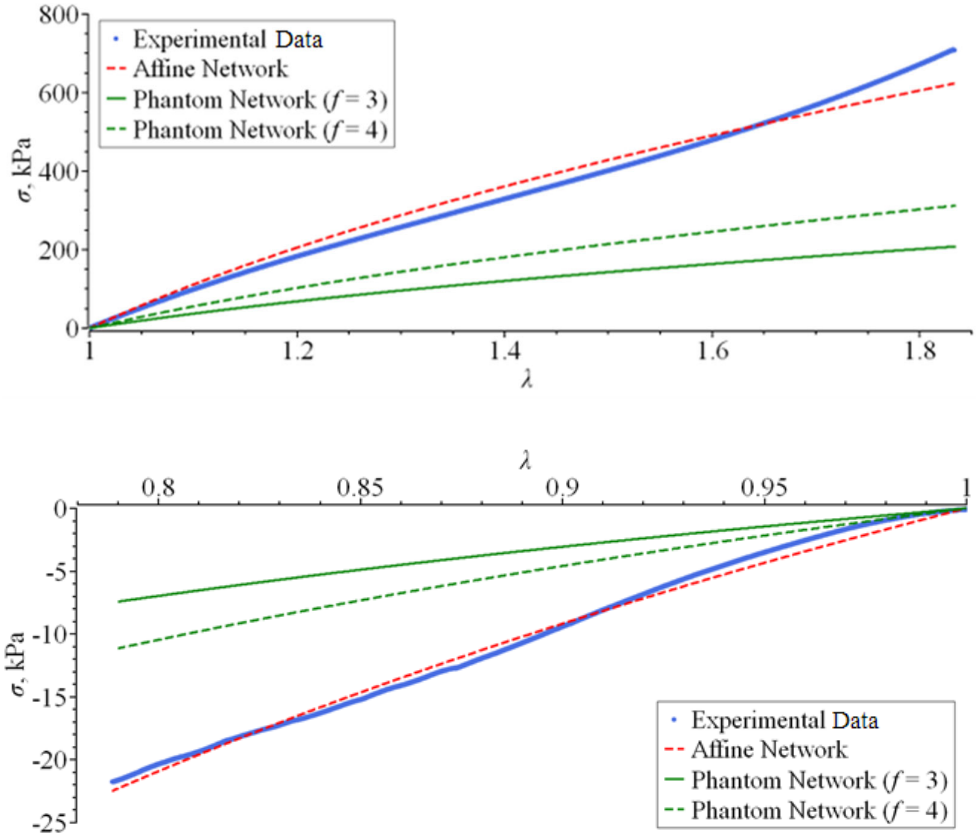

Figure 1. The stress–strain equations of the *affine* and *phantom* network models are matched against the experimental (blue lines) tensile (**above**) and compression (**below**) stress–strain curves of the LE-M rubber at 30 °C.

3.4. The Constrained Junction Models

The disagreement between the experimental data and the predictions of the phantom and affine models contributed to the most interesting advances in the theories of rubber elasticity introduced after 1975. These approaches, known as *constrained network* models, take into account the contributions of trapped entanglements to the elasticity of the network [8,17,29,31–34].

Among the models that attempt to account for the effect of topological constraints on active chains are constrained junction models. They are based on the initial work of Allegra and Ronca [35], later developed in the theories of Flory and Erman [36–39].

The presence of entanglements diminishes the fluctuations of junctions closer to the affine model's assumptions, whereas the increase in deformation decreases the density of the chains around a given junction, and therefore the range of fluctuations is closer to that of the phantom model. This effect is modeled by a harmonic potential acting on the junction points of the phantom network, then reducing the fluctuations of the active chains by restricting the motions of the cross-links. The constraining potential can be represented by confining the virtual chains' connecting junction points to the elastic background (Scheme 6).

The space available for chain fluctuations changes as a result of network deformations, as chains move further apart or closer together. To take this effect into account, the confining potential acting on the cross-links is assumed to change with the network deformation. Thus, the fluctuations of the virtual chains deform affinely with the network deformation. In both theories, the effects of the constraints are local and decrease with increasing strain; the difference between the two theories is that, in the Ronca–Allegra theory, the fluctuations of junctions become exactly affine as the undeformed state is approached; on the other hand, in the Flory–Erman theory, they are close to but below those of the affine state. In the approach of Ronca–Allegra [35] (Scheme 7), the ratio between the fluctuations along two directions would equal that between the corresponding stretch ratio—$s_x/s_y = \lambda_x/\lambda_y$—but no assumption was made on the magnitude of fluctuations. The engineering stress, referring to a uniaxial tension test, reads as follows:

$$\sigma_{\mathrm{R-A}} = \frac{\mu f k T}{2}\left(1 + \frac{2}{f}\frac{3\lambda}{\lambda^3 + 2}\right)\left(\lambda - \frac{1}{\lambda^2}\right) \tag{6}$$

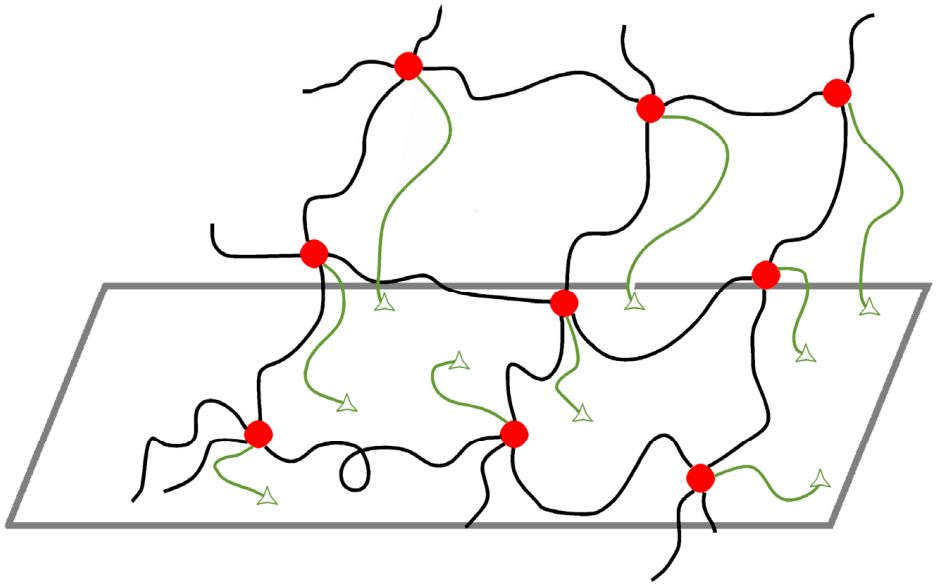

Scheme 6. Picture of the *Constrained junction model*. The virtual chains (green lines) connecting each network cross-link (red junction) to the elastic background (at the green triangles).

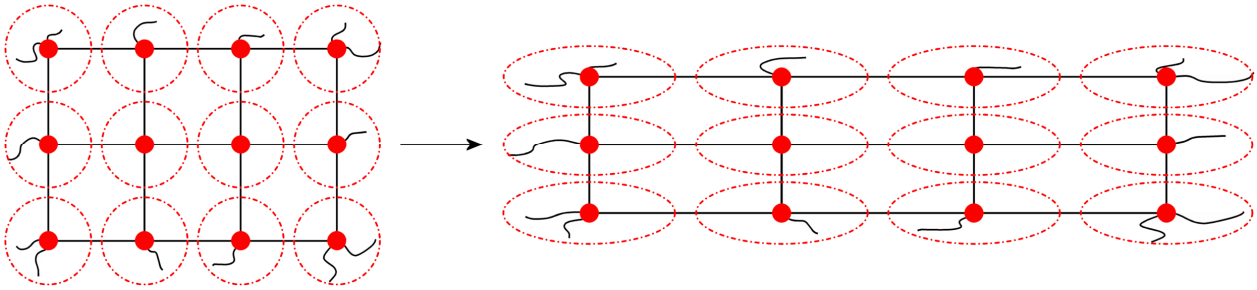

Scheme 7. Picture of the *Ronca–Allegra model*. The lattice deforms in an affine way and the fluctuation ellipsoids deform in a proportional way to the stretching of the lattice. The affine deformations $\lambda_x = 2$ and $\lambda_y = \lambda_z = 1/\sqrt{2}$ have been applied.

The stress of the constrained models takes the general form that follows:

$$\sigma = \sigma_{\mathrm{ph}}(1 + f_{\mathrm{cnstr}}(\lambda)) \tag{7}$$

where f_{cnstr} takes into account steric hindrances to the Brownian motion of the network.

The engineering stress of the *Flory–Erman model* is given by the work of [40,41].

$$\sigma_{c-j} = \sigma_{ph}\left[1 + \frac{2}{f-2}\frac{\lambda K(\lambda^2) - \lambda^{-2}K(\lambda^{-1})}{\lambda - \lambda^{-2}}\right] \quad (8)$$

where K is the trace of the stress tensor (i.e., the sum of the principal stresses) for an uniaxial deformed network.

In Figure 2, the stress–strain equations of the affine network and Ronca–Allegra models are matched against the experimental curves of the LE-M elastomer in tension or compression modes: the stress–strain curves for low deformations overlap perfectly.

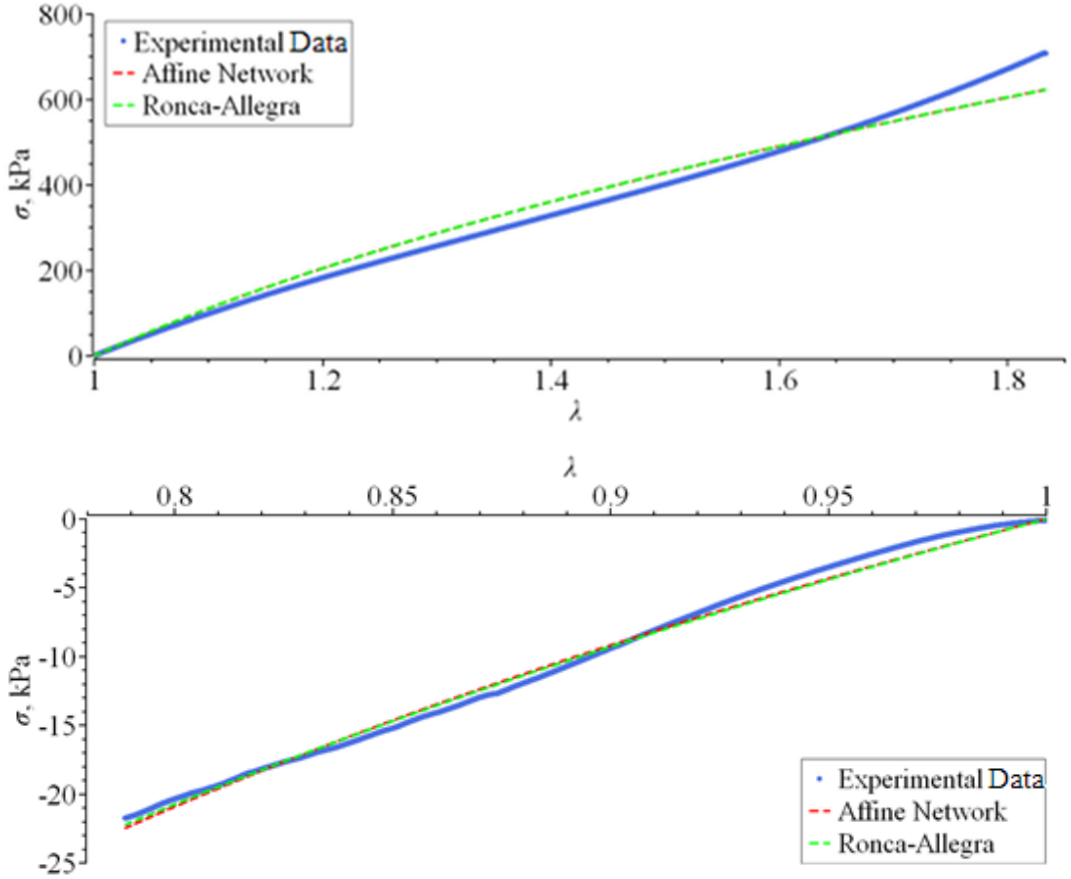

Figure 2. Comparison of the *Affine* and *Ronca–Allegra* models with experimental data of the LE-M rubber at 30 °C: the stress–strain equations of the models are matched against the experimental (blue lines) tensile (**above**) or compression (**below**) states for the LE-M rubber at 30 °C.

At the limit of a very strong potential, although the fluctuations of the junctions are completely suppressed, other monomers of the chain are not constrained and their fluctuations are almost unchanged. This is an unrealistic representation of topological interactions in polymer networks. The constrained junction model was revised in the constrained chain model, in which one considers the effects of the constraints on the centers of mass of the network chains [42–44]. Nevertheless, it is still not sufficient to represent the real topological interactions among the chains. A more realistic theory, the *Diffused constraint model*, considers the constraints affecting not only the fluctuations of junctions or mass centers but the fluctuations of all atoms along the chain backbone [45].

The main drawback of the constrained junction models is that they impose only limited constraints on chain fluctuations. Thus, they can only represent the crossover

between the phantom and affine models, that is, between weak constraining and strong constraining potentials.

3.5. The Tube Models

A more realistic model, the *Edwards tube model* [46,47], assumes permanent entanglements imposed along the whole backbone by the surrounding chains and restricts the fluctuations of all the monomers of the active chains (Scheme 8). The topological constraints are represented by the potential applied to all monomers, restricting their fluctuations to a confining tube. This potential is independent of network deformations and can be represented by virtual chains connecting network monomers to the elastic background.

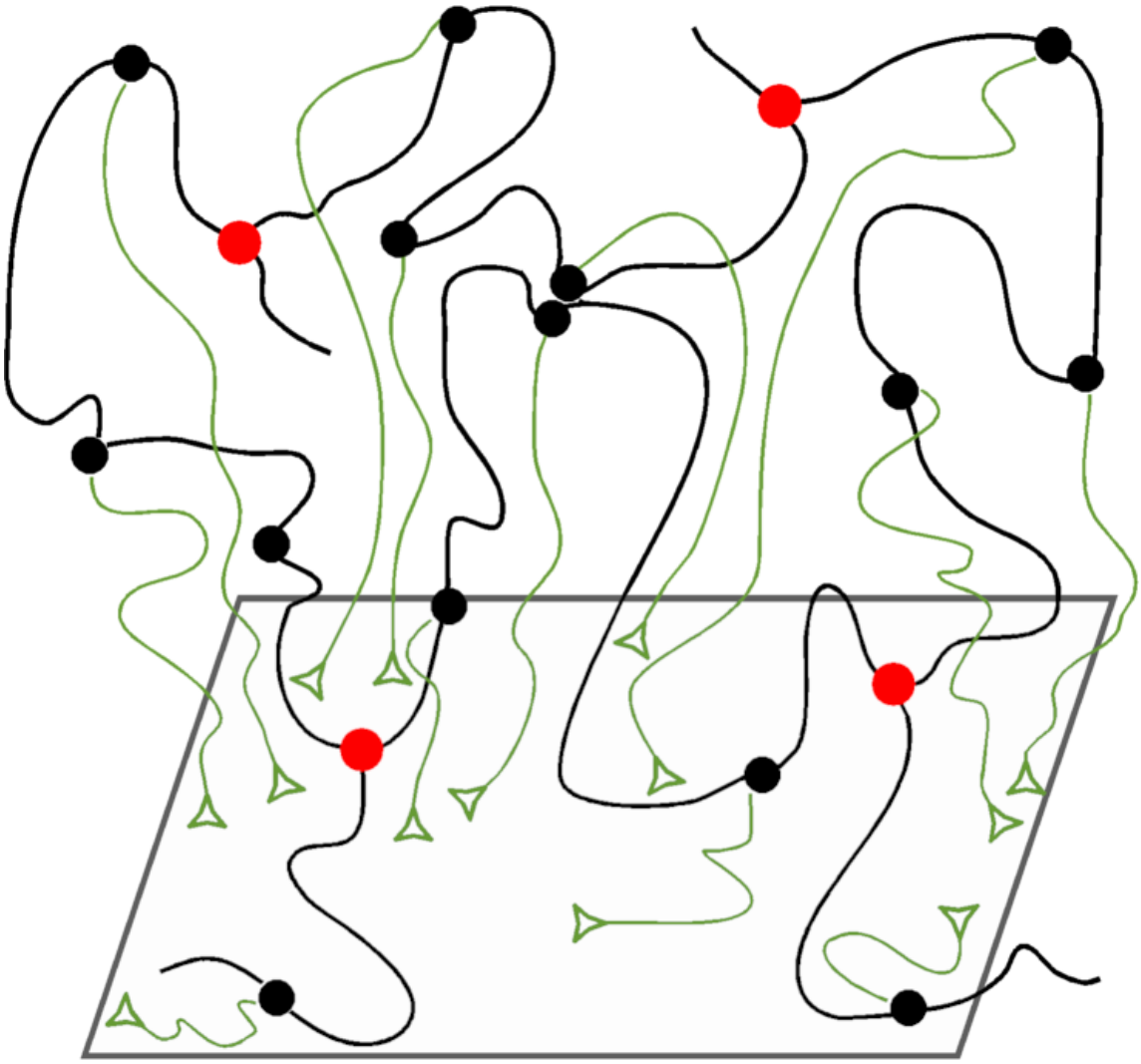

Scheme 8. Picture of the *Edwards tube model*. Each monomer of the network chains (black segments) is connected to the elastic background by virtual chains (green lines).

The stress–strain constitutive equation for this model is as follows:

$$\sigma_{E-t} = kT\frac{c}{N_e}\left(\lambda - \frac{1}{\lambda^2}\right) \quad (9)$$

where c is the monomer concentration and N_e is the number of monomers between entanglements; then, c/N_e is the entanglement density. Edwards' equation is analogous to that of the affine or phantom models and takes into account a cross-link density in the modulus G.

In tube models, the confining potential acting on a given network strand is assumed to be formed collectively by many neighboring active chains; this justifies the use of the mean-field description of topological entanglements.

Various tube models have been developed. In the *Marrucci tube model* [15] (Scheme 9), the engineering stress is calculated by assuming that the tube constraints deform affinely from the circular to the ellipsoidal cross-section:

$$\sigma_{\mathrm{M-t}} = \frac{l_0}{a_0}\nu kT\left(\frac{2}{3}+\frac{r}{3}\left(\frac{\lambda^2+2\lambda^{-1}}{3}\right)^{-\frac{1}{2}}\right)\left(\lambda-\frac{1}{\lambda^2}\right) \tag{10}$$

where a_0 is the tube radius of the uncross-linked polymer; a_r is the tube radius into an undeformed network ($a_\mathrm{r} \geq a_0$); $r = a_0^2/a_\mathrm{r}^2 \leq 1$ indicates the structural difference of the network with respect to the parent polymer; and l_0 is the contour length of the tubes.

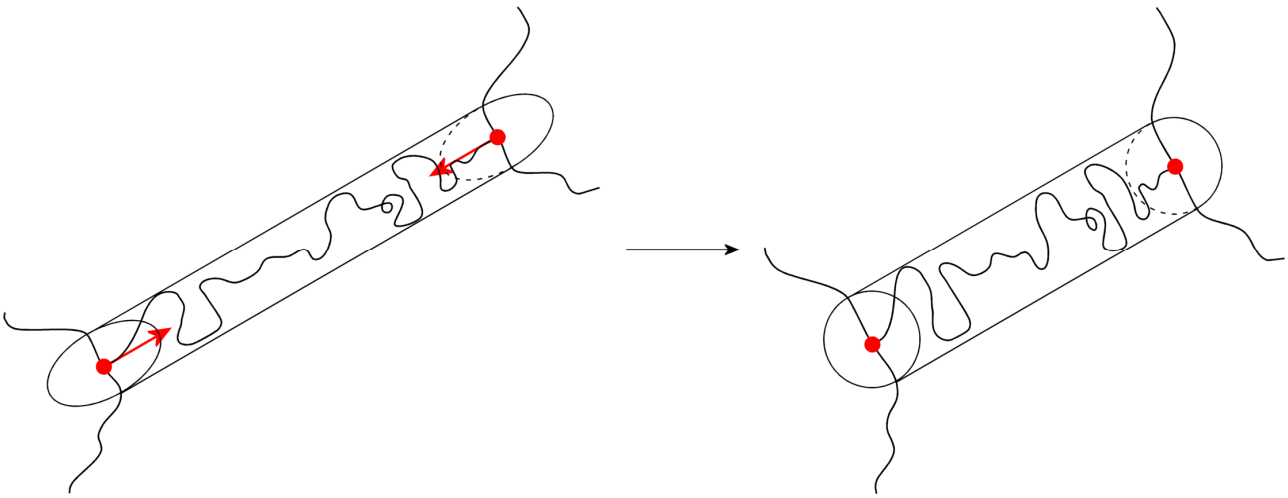

Scheme 9. Picture of the *Marrucci tube* model: the stretched network chain from the relaxed to the unstretched state. Each active chain is constrained inside a tube defined by the entanglements with the neighboring chains and deform affinely from the circular to the ellipsoidal cross-section.

Equation (10) differs from Equation (2) of the affine model by the presence of an amplifying factor of the network modulus; it gives a valid description of tensile behavior, but in compression it predicts too much softening [48].

3.6. The Slip-Link Models

In *Slip-link models*, the trapped entanglement is simulated by a pair of chains that slide through a virtual ring (i.e., the slip-link), separated from each other by the tube diameter. Then, the slip-links may move along the network chain when a deformation is applied to the network. The cross-linking leads to permanent topological constraints, so a slip-link acts as if it were an additional cross-link. Therefore, the slip-link model of Edwards and Vilgis [49] uses the tube model of polymer melts to predict that entanglements will increase the value of the modulus G over that predicted by the phantom model (Scheme 10).

Their predictions for the modulus are consistent with the experiments, and empirical fits to these results represented by the sum of two terms:

$$G = G_\mathrm{ph} + G_\mathrm{N}^0 T_\mathrm{e} \tag{11}$$

where G_N^0 is the plateau modulus of the polymer melt and T_e is the trapped entanglement factor of Langley less or equal to unity [9,50,51]. The first term is the contribution of the chemical cross-links; the additional term $G_\mathrm{N}^0 T_\mathrm{e}$ is due to permanently trapped entangle-

ments in the network. Equation (11) is of general applicability and does not rely on any details of the entanglement model.

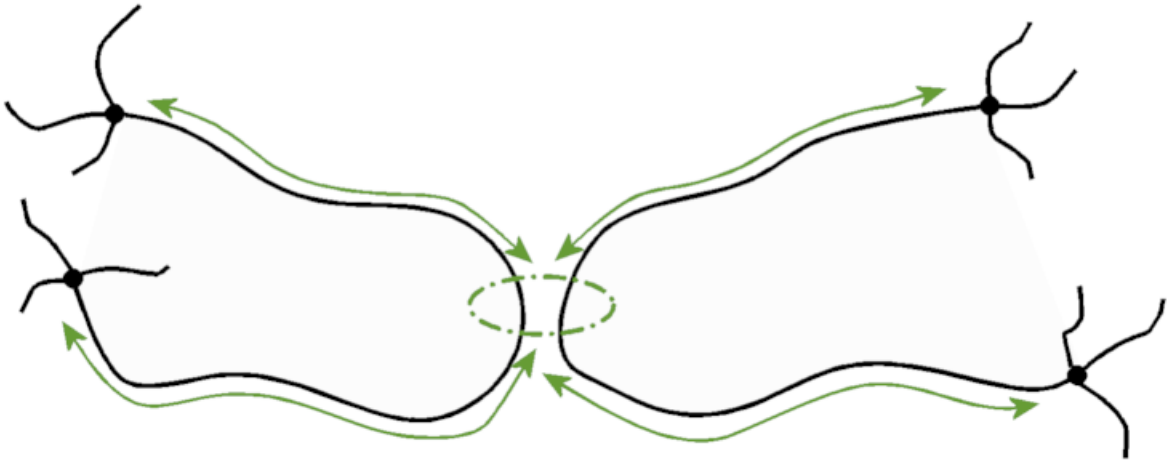

Scheme 10. Picture of the *Sip-link model*. The slip-link (the green dash–dotted circle) models a trapped entanglement joining two network chains and can move among the cross-links upon the rubber stretching.

Both the constrained junction and the slip-link models' free energies reduce to that of the phantom network when the effect of the entanglements tends to zero. One important difference between the two models, however, is that the constrained junction model's free energy equates to that of the affine network model at the limit of infinitely strong constraints, whereas the slip-link model's free energy may exceed that for an affine deformation [9].

3.7. The Nonaffine Tube Model

The *Nonaffine tube model* developed by Rubinstein and Panyukov [16] combines the main characteristics of the constrained junction and Edwards tube models.

In this model, the amplitude of fluctuations that defines the tube diameter changes proportionally with network deformations and the potential acts not only on junctions but also on the monomers of active chains. The most important feature of this model is that the tube diameter changes nonaffinely with macroscopic stretch ratios. The prediction for the engineering stress of the Nonaffine tube model is as follows:

$$\sigma_{na-t} = \left(G_{ph} + \frac{G_e}{\lambda - \lambda^{\frac{1}{2}} + 1}\right)\left(\lambda - \frac{1}{\lambda^2}\right) \quad (12)$$

where G_{ph} is the phantom modulus and G_e is the entanglement contribution to the modulus.

In the nonaffine tube model, there is no possibility of the sliding of the network chains and the redistribution of its monomers along the contour of the tube. The slippage mechanism of the chain along the contour of the tube was proposed by de Gennes [4] in the reptation model of polymer melts and leads to the main modes of stress relaxation in polymer melt reptation and tube length fluctuations. The analysis of the redistribution of the stored length along the tube contour was made by Doi [52]; in anisotropically deformed highly entangled networks, this redistribution will be important.

3.8. The Nonaffine Slip–Tube Model

A more advanced version of the model just described combines the features of tube and slip-link models in the slip–tube model of Rubinstein and Panyukov [17,53]. In this model, the constraints imposed by the neighboring active chains are modeled by virtual chains attached to the elastic background at one end and ending with slip-links at the other (Scheme 11). These slip-links can freely slide along the contour of the chains, but they are not allowed to pass through each other. Therefore, the amplitude of slip-link fluctuations

along the contour of the chain depends on the density of these links. At a high density, the fluctuations are suppressed and the model reduces to the nonaffine tube model. If slippage along the tube is allowed, the network chains redistribute their lengths along the contour of their confining tubes; as a result, this model accounts for the redistribution of monomers between different sections of the tube.

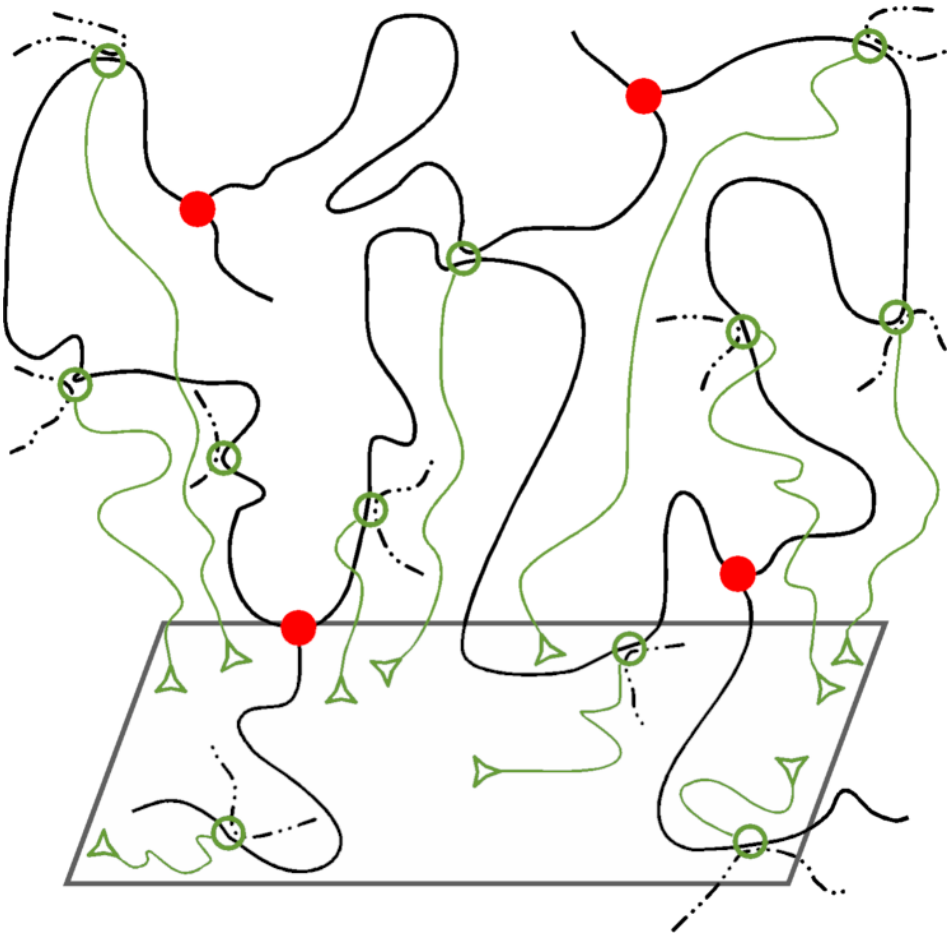

Scheme 11. Picture of the *Nonaffine slip–tube* model: the slip-links are attached to the elastic background by virtual chains that represent the potential of the confining tube.

The dependence of engineering stress on the deformation cannot be expressed as a closed-form expression. Nevertheless, the numerical solution of this model in the experimentally relevant range $0.1 < \lambda < 10$ can be well approximated by the following equation:

$$\sigma_{\text{na s-t}} = \left(G_{\text{ph}} + \frac{G_{\text{e}}}{0.74\lambda + 0.61\lambda^{-\frac{1}{2}} - 0.35}\right)\left(\lambda - \frac{1}{\lambda^2}\right) \quad (13)$$

By means of Equation (13), it is possible to separate the phantom and entanglement contributions to network elasticity, providing a reasonable description of the experimental data.

In Figure 3, the constitutive stress–strain equations of the Marrucci, Rubinstein–Panyukov, and Edwards–Vilgis models are matched against the experimental stress–strain curve of LE-M rubber. The Nonaffine, Slip and Marrucci tube models overlap in compression in excellent agreement with the experimental data. Conversely, in tension, the Marrucci tube model presents a substantial mismatch.

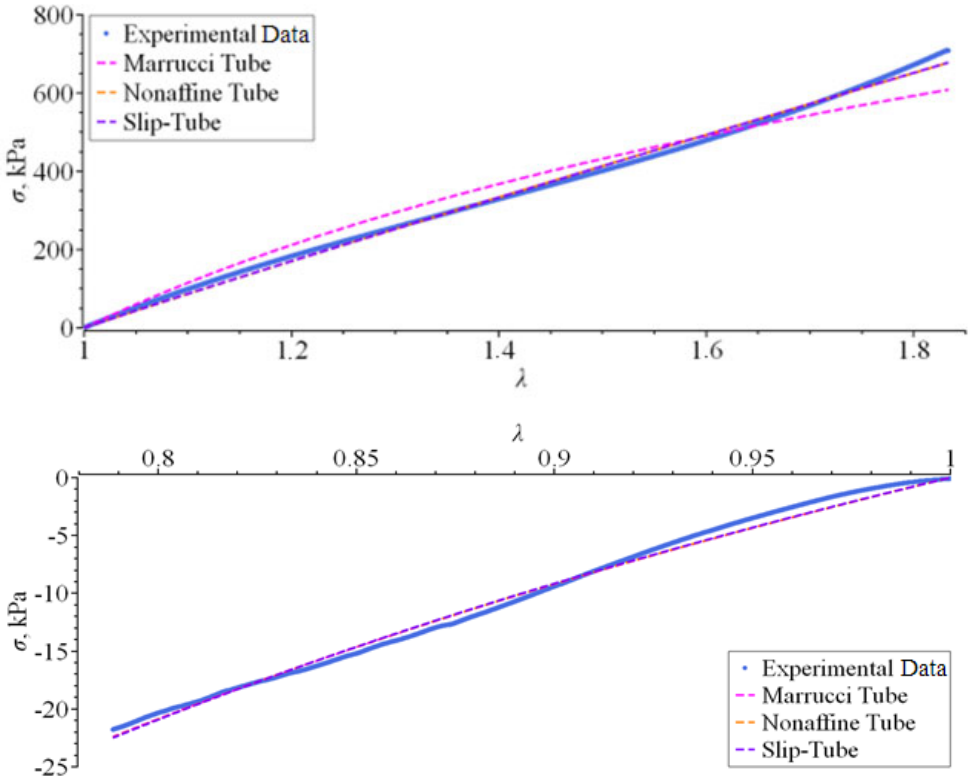

Figure 3. Comparison of the entanglement tube models against the experimental (blue lines) tensile (**above**) or compression (**below**) stress–strain curves for the LE-M rubber at 30 °C.

3.9. The Mooney–Rivlin Models

The theories of rubber elasticity described so far are based on a molecular approach: although they account for the stretching of the rubber up to $\lambda = 2$ (i.e., $\varepsilon = 100\%$), they do not satisfactorily account for the stress–strain curve in the whole span of deformations. In order to fit the experimental data, a different approach from the molecular models is based on phenomenological models, considering the elastomer as a continuum [54–56]. One of the successful phenomenological treatments is the semiempirical Mooney–Rivlin model, which is in agreement with the experimental data up to $\lambda = 4$ (i.e., $\varepsilon = 300\%$) [18,19,57]. At rest, the network is considered isotropic and incompressible and is assumed to behave like a Hookean material upon shearing. The authors proposed the following constitutive expression for the engineering stress:

$$\sigma_{M-R} = 2\left(C_1 + \frac{C_2}{\lambda}\right)\left(\lambda - \frac{1}{\lambda^2}\right) \quad (14)$$

where C_1 and C_2 are coefficients that vary with the material under consideration and its molecular characteristics. Contrary to the molecular models, the stress is supposed to vary with the deformation applied. Equation (14) coincides with Equation (2) of the affine network model, setting $2C_1 = kT\nu$ and $C_2 = 0$. The values of the coefficient C_2 increase in the presence of entanglements and at a low deformation. To the contrary, C_2 is close to zero for highly swollen networks or by going to high temperatures to reach an equilibrium deformation; as a result, this coefficient could be caused by the nonaffine deformation of the entanglement network [58]. Therefore, even though Equation (14) fits the stress–strain curve for an elastomer under practical conditions, Equation (2) remains valid for a network at equilibrium under an applied load.

By increasing the number of parameters, the predictive accuracy of the fitting by the Mooney–Rivlin model increases. Equation (2) represents the two-parameter Mooney–Rivlin equation. As a general rule, if the rubber stress–strain curve has a single curvature (i.e., no

inflection points), then Equation (2) is suitable, whereas if one or two inflection points are present, then the five- or nine-parameter equations should be utilized [59–61].

In this present paper, the Mooney–Rivlin model in the two-, three-, or five-parameter form proves appropriate for the LE-M rubber, as we can see from the goodness of fit shown in Figure 4. The engineering stress for the three- and five-parameter Mooney–Rivlin model is given by the following:

$$\sigma_{3-\mathrm{p\ M-R}} = 2C_1\left(\lambda - \frac{1}{\lambda^2}\right) + 2C_2\left(1 - \frac{1}{\lambda^3}\right) + 6C_3\left(\lambda^2 - \lambda - 1 + \frac{1}{\lambda^2} + \frac{1}{\lambda^3} - \frac{1}{\lambda^4}\right) \quad (15)$$

$$\begin{aligned}\sigma_{5-\mathrm{p\ M-R}} = {} & 2C_1\left(\lambda - \tfrac{1}{\lambda^2}\right) + 2C_2\left(1 - \tfrac{1}{\lambda^3}\right) + 6C_3\left(\lambda^2 - \lambda - 1 + \tfrac{1}{\lambda^2} + \tfrac{1}{\lambda^3} - \tfrac{1}{\lambda^4}\right) \\ & + 4C_4\lambda\left(1 - \tfrac{1}{\lambda^3}\right)\left(\lambda^2 + \tfrac{2}{\lambda} - 3\right) \\ & + 4C_5\left(2\lambda + \tfrac{1}{\lambda^2} - 3\right)\left(1 - \tfrac{1}{\lambda^3}\right)\end{aligned} \quad (16)$$

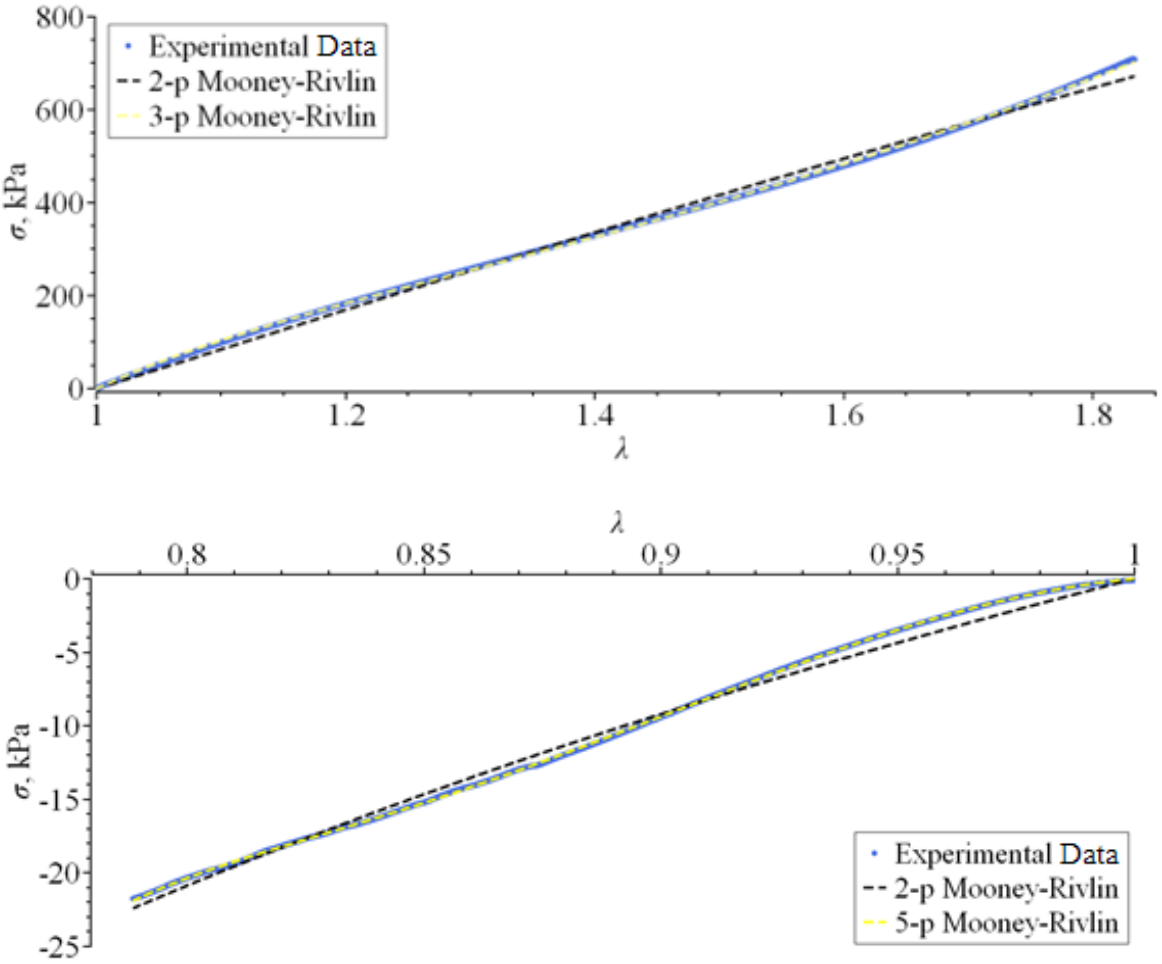

Figure 4. Comparison of the two-, three-, and five-parameter (2-p, 3-p, and 5-p) Mooney–Rivlin equations against the experimental (blue lines) tensile (**above**) or compression (**below**) stress–strain curves for the LE-M rubber at 30 °C.

Now, we compare our outcome to the various models of rubber elasticity by means of nonlinear curve fitting. Tables 1 and 2 summarize the constitutive stress–strain equations of the models analyzed in tension and in compression, respectively, reporting the *coefficient of determination* R^2.

Table 1. Comparison of constitutive stress–strain equations and R^2 determination coefficient in tensile fitting.

Model	Constitutive Stress–Strain Equation	R^2
Affine Network	$\sigma_{\text{aff}} = kTv\left(\lambda - \frac{1}{\lambda^2}\right)$	0.97608
Ronca–Allegra	$\sigma_{\text{R-A}} = \frac{\mu f k T}{2}\left(1 + \frac{2}{f}\frac{3\lambda}{\lambda^3+2}\right)\left(\lambda - \frac{1}{\lambda^2}\right)$	0.97608
Marrucci Tube (r = 1)	$\sigma_{\text{M-t}} = \frac{l_0}{a_0}\nu k T\left(\frac{2}{3} + \frac{r}{3}\left(\frac{\lambda^2+2\lambda^{-1}}{3}\right)^{-\frac{1}{2}}\right)\left(\lambda - \frac{1}{\lambda^2}\right)$	0.96526
Nonaffine Tube	$\sigma_{\text{na-t}} = \left(G_{\text{ph}} + \frac{G_{\text{e}}}{\lambda - \lambda^{\frac{1}{2}} + 1}\right)\left(\lambda - \frac{1}{\lambda^2}\right)$	0.99649
Nonaffine Slip–Tube	$\sigma_{\text{na s-t}} = \left(G_{\text{ph}} + \frac{G_{\text{e}}}{0.74\lambda + 0.61\lambda^{-\frac{1}{2}} - 0.35}\right)\left(\lambda - \frac{1}{\lambda^2}\right)$	0.99663
Two-parameter Mooney–Rivlin	$\sigma_{\text{2-p M-R}} = 2\left(C_1 + \frac{C_2}{\lambda}\right)\left(\lambda - \frac{1}{\lambda^2}\right)$	0.99531
Three-parameter Mooney–Rivlin	$\sigma_{\text{3-p M-R}} = 2C_1\left(\lambda - \frac{1}{\lambda^2}\right) + 2C_2\left(1 - \frac{1}{\lambda^3}\right) + 6C_3\left(\lambda^2 - \lambda - 1 + \frac{1}{\lambda^2} + \frac{1}{\lambda^3} - \frac{1}{\lambda^4}\right)$	0.99978

Table 2. Comparison of constitutive stress–strain equations and R^2 determination coefficient in compression fitting.

Model	Stress–Strain Constitutive Equation	R^2
Affine Network	$\sigma_{\text{aff}} = kTv\left(\lambda - \frac{1}{\lambda^2}\right)$	0.99299
Ronca–Allegra	$\sigma_{\text{R-A}} = \frac{\mu f k T}{2}\left(1 + \frac{2}{f}\frac{3\lambda}{\lambda^3+2}\right)\left(\lambda - \frac{1}{\lambda^2}\right)$	0.99317
Marrucci Tube (r = 1)	$\sigma_{\text{M-t}} = \frac{l_0}{a_0}\nu k T\left(\frac{2}{3} + \frac{r}{3}\left(\frac{\lambda^2+2\lambda^{-1}}{3}\right)^{-\frac{1}{2}}\right)\left(\lambda - \frac{1}{\lambda^2}\right)$	0.99308
Nonaffine Tube	$\sigma_{\text{na-t}} = \left(G_{\text{ph}} + \frac{G_{\text{e}}}{\lambda - \lambda^{\frac{1}{2}} + 1}\right)\left(\lambda - \frac{1}{\lambda^2}\right)$	0.99299
Nonaffine Slip–Tube	$\sigma_{\text{na s-t}} = \left(G_{\text{ph}} + \frac{G_{\text{e}}}{0.74\lambda + 0.61\lambda^{-\frac{1}{2}} - 0.35}\right)\left(\lambda - \frac{1}{\lambda^2}\right)$	0.99299
Two-parameter Mooney–Rivlin	$\sigma_{\text{2-p M-R}} = 2\left(C_1 + \frac{C_2}{\lambda}\right)\left(\lambda - \frac{1}{\lambda^2}\right)$	0.99301
Five-parameter Mooney–Rivlin	$\sigma_{\text{5-p M-R}} = 2C_1\left(\lambda - \frac{1}{\lambda^2}\right) + 2C_2\left(1 - \frac{1}{\lambda^3}\right) + 6C_3\left(\lambda^2 - \lambda - 1 + \frac{1}{\lambda^2} + \frac{1}{\lambda^3} - \frac{1}{\lambda^4}\right) + 4C_4\lambda\left(1 - \frac{1}{\lambda^3}\right)\left(\lambda^2 + \frac{2}{\lambda} - 3\right) + 4C_5\left(2\lambda + \frac{1}{\lambda^2} - 3\right)\left(1 - \frac{1}{\lambda^3}\right)$	0.99994

The fitting of the tension curves shows a differentiation between the several models. In particular, the Affine network, Ronca–Allegra, and Marrucci tube models show a fair match with the experimental data. Conversely, in good agreement with the literature [53,62–64], the Nonaffine tube and Two-parameter Mooney–Rivlin models meet the experimental curve up to λ = 2 in a very satisfactory way. An increase in the fitting parameters of the Mooney–Rivlin phenomenological model, precisely three parameters, leads to an improvement in the agreement with the experimental data.

At high elongations, the experimental data show an upturn, thus deviating significantly from the Mooney–Rivlin equation. Furthermore, the compression data depart from the Mooney–Rivlin prediction [34]. However, the two-parameter Mooney–Rivlin model has proven accurate up to 100% strain in tension and 30% strain in compression, and, using a higher parameter model, it may provide better results at higher strains [59].

By analyzing the fitting of the stress–strain curves in compression, we observe the same good agreement with the experimental data. This highlights the goodness of the early molecular models in interpreting the stress–strain curve at a low deformation. Furthermore,

the five-parameter M-R model even leads to an excellent fit of the curve in the whole experimental strain range.

4. Conclusions

A rubber network is a system of cross-linked polymer chains that experience the entropic elastic force of Brownian motions and confined diffusion due to covalent and topological constraints; in general, it is a complex n-body system irreducibly nonlinear. The ideal models originally developed consider a set of mutually independent Gaussian coils, the entropic springs, interconnected by cross-links. To take into account the restraints imposed by the intermolecular couplings of the entanglements, constrained, tube, and slip-link models of increasing complexity have been proposed, improving the theoretical predictions. A fundamental difficulty lies in the non-hierarchical topology of the rubber network characterized by a Gaussian distribution of active strand lengths. Therefore, long-range active chains between sites far away occur and necessarily involve the formation of an entangled network with trapped entanglements of varying complexity, the contribution of which becomes essential to large deformations. The most advanced models take into account such difficulty from a statistical and dynamic point of view, treating the contribution of sliding links as perturbations on the related entropic primary effects. Furthermore, recent advances by Olsten, Johnson, and Lang have made it possible to take into account the ends, loops, defects, and complex connectivity present in a real rubber network.

The analysis of the reviewed models highlights the goodness of the theories in describing the elastic behavior for deformations not excessively high up. The affine deformation models describe the compression experiments up to $\lambda \leq 1$ but do not describe the tension data up to $\lambda \leq 2$. In contrast, nonaffine and phenomenological models describe well both tension and compression experiments; this highlights that the affine deformation hypothesis is rigorously verified only for deformations $\lambda \leq 1$.

Further issues remain open: the deviations from the Gaussian distribution of network chains in real rubber (1); the crucial role of the entanglement density in experimental conditions (2); the experimental validation of the effect of virtual chains (3); the computational complexity of the Slip–tube model (4); how the transformation of specific molecular orbitals and elasticity are connected (5). Recently, theories and experiments of rubber elasticity on hydrogel networks characterized by non-Gaussian end-to-end distribution have been elaborated [65–67].

The literature on the theories of rubber elasticity is huge and often nebulous to a large audience. We believe that this review with original experimental data brings a contribution of clarity on the state of the art and can be a way of celebrating the 90-year anniversary of Kuhn's first theory of macromolecular chemistry [2].

Funding: This research received no external funding.

Acknowledgments: I thank the anonymous referees for their stimulating and valuable suggestions.

Conflicts of Interest: The authors declare no conflict of interest.

References

1. Staudinger, H. Über Polymerisation. *Ber. Dtsch. Chem. Ges.* **1920**, *53*, 1073–1085. [CrossRef]
2. Kuhn, W. Über die Gestalt fadenförmiger Moleküle in Lösungen. *Kolloid Zeitschrift* **1934**, *68*, 2–15. [CrossRef]
3. Kuhn, W. Dependence of the Average Transversal on the Longitudinal Dimensions of Statistical Coils Formed by Chain Molecules. *J. Polym. Sci.* **1946**, *1*, 380–388. [CrossRef]
4. de Gennes, P.-G. *Scaling Concepts in Polymer Physics*; Cornell University Press: Ithaca, NY, USA, 1979.
5. Grizzuti, N. *Reologia dei Materiali Polimerici: Scienza ed Ingegneria*; Edizioni Nuova Cultura: Roma, Italy, 2012.
6. Villani, V. *Introduzione alla Scienza dei Materiali Polimerici*; Aracne Editrice: Roma, Italy, 2017.
7. Treloar, L.R.G. *The Physics of Rubber Elasticity*, 3rd ed.; Oxford University Press: Oxford, UK, 1975.
8. Mark, J.E. *Physical Properties of Polymers Handbook*, 2nd ed.; Springer: New York, NY, USA, 2007.
9. Mark, J.E.; Erman, B.; Roland, C.M. *The Science and Technology of Rubber*, 4th ed.; Elsevier Academic Press: Waltham, MA, USA, 2013.
10. Erman, B.; Mark, J.E. *Structure and Properties of Rubberlike Networks*; Oxford University Press: New York, NY, USA, 1997.
11. Ali, A.; Hosseini, M.; Sahari, B.B. A review and comparison on some rubber elasticity models. *J. Sci. Ind. Res.* **2010**, *69*, 495–500.

12. Gedde, U.W.; Hedenqvist, M.S. *Fundamental Polymer Science*, 2nd ed.; Springer: Cham, Switzerland, 2019.
13. Zhong, M.; Wang, R.; Kawamoto, K.; Olsen, B.D.; Johnson, J.A. Quantifying the impact of molecular defects on polymer network elasticity. *Science* **2016**, *353*, 1264–1268. [CrossRef]
14. Lin, T.-S.; Wang, R.; Johnson, J.A.; Olsen, B.D. Revisiting the Elasticity Theory for Real Gaussian Phantom Networks. *Macromolecules* **2019**, *52*, 1685–1694. [CrossRef]
15. Marrucci, G. Rubber Elasticity Theory. A Network of Entangled Chains. *Macromolecules* **1981**, *14*, 434–442. [CrossRef]
16. Rubinstein, M.; Panyukov, S.V. Nonaffine Deformation and Elasticity of Polymer Networks. *Macromolecules* **1997**, *30*, 8036–8044. [CrossRef]
17. Rubinstein, M.; Panyukov, S. Elasticity of Polymer Networks. *Macromolecules* **2002**, *35*, 6670–6686. [CrossRef]
18. Mooney, M. The Thermodynamics of a Strained Elastomer. I. General Analysis. *J. Appl. Phys.* **1948**, *19*, 434–444. [CrossRef]
19. Rivlin, R.S.; Rideal, E.K. Large elastic deformations of isotropic materials IV. Further developments of the general theory. *Philos. Trans. R. Soc. A* **1948**, *241*, 379–397.
20. Villani, V.; Lavallata, V. Unusual Rheological Properties of Lightly Crosslinked Polydimethylsiloxane. *Macromol. Chem. Phys.* **2017**, *218*, 1700037. [CrossRef]
21. Villani, V.; Lavallata, V. Unexpected Rheology of Polydimethylsiloxane Liquid Blends. *Macromol. Chem. Phys.* **2018**, *219*, 1700623. [CrossRef]
22. Villani, V.; Lavallata, V. Entanglement Locking in the Unique Elasticity of Polydimethylsiloxane Rubbers. *Macromol. Chem. Phys.* **2020**, *221*, 1900497. [CrossRef]
23. Elias, H.-G.; Mülhaupt, R. *Ullmann's Polymers and Plastics*; Wiley-VCH: Weinheim, Germany, 2016.
24. Wall, F.T.; Flory, P.J. Statistical Thermodynamics of Rubber Elasticity. *J. Chem. Phys.* **1951**, *19*, 1435–1439. [CrossRef]
25. Flory, P.J. Statistical thermodynamics of random networks. *Proc. R. Soc. Lond. A* **1976**, *351*, 351–380.
26. James, H.M.; Guth, E. Theory of the Elastic Properties of Rubber. *J. Chem. Phys.* **1943**, *11*, 455–481. [CrossRef]
27. James, H.M. Statistical Properties of Networks of Flexible Chains. *J. Chem. Phys.* **1947**, *15*, 651–668. [CrossRef]
28. James, H.M.; Guth, E. Theory of the Increase in Rigidity of Rubber during Cure. *J. Chem. Phys.* **1947**, *15*, 669–683. [CrossRef]
29. Halary, J.L.; Laupretre, F.; Monnerie, L. *Polymer Materials Macroscopic Properties and Molecular Interpretations*; Wiley: New York, NY, USA, 2011.
30. Lang, M. Relation between Cross-Link Fluctuations and Elasticity in Entangled Polymer Networks. *Macromolecules* **2017**, *50*, 2547–2555. [CrossRef]
31. Mark, J.; Ngai, K.; Graessley, W.; Mandelkern, L.; Samulski, E.; Koenig, J.; Wignall, G. *Physical Properties of Polymers*, 3rd ed.; Cambridge University Press: Cambridge, UK, 2004.
32. Saccomandi, G.; Ogden, R.W. *Mechanics and Thermomechanics of Rubberlike Solids*; Springer: Wien, Austria, 2004.
33. Mark, J.E.; Erman, B. *Rubberlike Elasticity a Molecular Primer*, 2nd ed.; Cambridge University Press: Cambridge, UK, 2007.
34. *Properties and Behavior of Polymers*; Wiley: Hoboken, NJ, USA, 2011.
35. Ronca, G.; Allegra, G. An approach to rubber elasticity with internal constraints. *J. Chem. Phys.* **1975**, *63*, 4990–4997. [CrossRef]
36. Erman, B.; Flory, P.J. Theory of elasticity of polymer networks. II. The effect of geometric constraints on junctions. *J. Chem. Phys.* **1978**, *68*, 5363–5369. [CrossRef]
37. Flory, P.J. Molecular Theory of Rubber Elasticity. *Polym. J.* **1985**, *17*, 1317–1320. [CrossRef]
38. Flory, P.J. Network topology and the theory of rubber elasticity. *Br. Polym. J.* **1985**, *17*, 96–102. [CrossRef]
39. Erman, B.; Mark, J.E. Rubber-like Elasticity. *Ann. Rev. Phys. Chem.* **1989**, *40*, 351–374. [CrossRef]
40. Flory, P.J. Theory of elasticity of polymer networks. The effect of local constraints on junctions. *J. Chem. Phys.* **1977**, *66*, 5720–5729. [CrossRef]
41. Roland, C.M. *Viscoelastic Behavior of Rubbery Materials*; Oxford University Press: Oxford, UK, 2011.
42. Erman, B.; Monnerie, L. Theory of elasticity of amorphous networks: Effect of constraints along chains. *Macromolecules* **1989**, *22*, 3342–3348. [CrossRef]
43. Fontaine, F.; Noel, C.; Monnerie, L.; Erman, B. Stress-strain-swelling behaviour of amorphous polymeric networks: Comparison of experimental data with theory. *Macromolecules* **1989**, *22*, 3352–3355. [CrossRef]
44. Erman, B.; Monnerie, L. Theory of Elasticity of amorphous networks: Effects of Constraints along Chains. *Macromolecules* **1992**, *25*, 4456. [CrossRef]
45. Kloczkowski, A.; Mark, J.E.; Erman, B. A Diffused-Constraint Theory for the Elasticity of Amorphous Polymer Networks. 1. Fundamentals and Stress-Strain Isotherms in Elongation. *Macromolecules* **1995**, *28*, 5089–5096. [CrossRef]
46. Edwards, S.F. The statistical mechanics of polymerized material. *Proc. Phys. Soc.* **1967**, *92*, 9–16. [CrossRef]
47. Edwards, S.F.; Vilgis, T.A. The tube model theory of rubber elasticity. *Rep. Prog. Phys.* **1988**, *51*, 243–297. [CrossRef]
48. Graessley, W.W. *Polymeric Liquids & Networks: Structure and Properties*; Garland Science: New York, NY, USA, 2004.
49. Edwards, S.F.; Vilgis, T.A. The effect of entanglements in rubber elasticity. *Polymer* **1986**, *27*, 483–492. [CrossRef]
50. Dossin, L.M.; Graessley, W.W. Rubber Elasticity of Well-Characterized Polybutadiene Networks. *Macromolecules* **1979**, *12*, 123–130. [CrossRef]
51. Queslel, J.P.; Mark, J.E. *Encyclopedia of Polymer Science and Technology*; Mark, H.F., Ed.; Wiley: Hoboken, NJ, USA, 2014.
52. Doi, M. Explanation for the 3.4-power law for viscosity of polymeric liquids on the basis of the tube mode. *J. Polym. Sci. Polym. Phys. Ed.* **1983**, *21*, 667–684. [CrossRef]

53. Rubinstein, M.; Colby, R.H. *Polymer Physics*; Oxford University Press: Oxford, UK, 2003.
54. Bueche, F. *Physical Properties of Polymers*; Interscience Publishers: New York, NY, USA, 1962.
55. Sperling, L.H. *Introduction to Physical Polymer Science*, 4th ed.; Wiley: Hoboken, NJ, USA, 2006.
56. Gnanou, Y.; Fontanille, M. *Organic and Physical Chemistry of Polymers*; Wiley: Hoboken, NJ, USA, 2008.
57. Mooney, M. A Theory of Large Elastic Deformation. *J. Appl. Phys.* **1940**, *11*, 582–592. [CrossRef]
58. Wagner, M.H. The origin of the C_2 term in rubber elasticity. *J. Rheol.* **1994**, *38*, 655–679. [CrossRef]
59. Donald, B.J.M. *Practical Stress Analysis with Finite Elements*; Glasnevin Publishing: Dublin, Ireland, 2007.
60. Kumar, N.; Rao, V.V. Hyperelastic Mooney-Rivlin Model: Determination and Physical Interpretation of Material Constants. *MIT Int. J. Mech. Eng.* **2016**, *6*, 43–46.
61. Szurgott, P.; Jarzębski, Ł. Selection of a Hyper-Elastic Material Model—A Case Study for Polyurethane Component. *Lat. Am. J. Solids Struct.* **2019**, *16*, e191. [CrossRef]
62. Svaneborg, C.; Everaers, R.; Grest, G.S.; Curro, J.G. Connectivity and Entanglement Stress Contributions in Strained Polymer Networks. *Macromolecules* **2008**, *41*, 4920–4928. [CrossRef]
63. Yoo, S.H.; Yee, L.; Cohen, C. Effect of network structure on the stress-strain behaviour of endlinked PDMS elastomers. *Polymer* **2010**, *51*, 1608–1613. [CrossRef]
64. Sliozberg, Y.R.; Mrozek, R.A.; Schieber, J.D.; Kröger, M.; Lenhart, J.L.; Andzelm, J.W. Effect of polymer solvent on the mechanical properties of entangled polymer gels: Coarse-grained molecular simulation. *Polymer* **2013**, *54*, 2555–2564. [CrossRef]
65. Wittmer, J.P.; Beckrich, P.; Meyer, H.; Cavallo, A.; Johner, A.; Baschnagel, J. Intramolecular long-range correlations in polymer melts: The segmental size distribution and its moments. *Phys. Rev. E* **2007**, *76*, 011803. [CrossRef] [PubMed]
66. Mezzasalma, S.A.; Abramic, M.; Grassi, G.; Grassi, M. Rubber Elasticity of Polymer Networks in Explicitly non-Gaussian States. Statistical Mechanics and LF-NMR Inquiry in Hydrogel Systems. *Int. J. Eng. Sci.* **2022**, *176*, 103676. [CrossRef]
67. Bock, W.; da Silva, J.L.; Streit, L. On the potential in non-Gaussian chain polymer models. *Math. Methods Appl. Sci.* **2019**, *42*, 7452–7460. [CrossRef]